Polymer 51 (2010) 4823–4830

Contents lists available at ScienceDirect

Polymer

journal homepage: www.elsevier.com/locate/polymer

Self-assembled, optically responsive nematic liquid crystal/polymer core-shell fibers: Formation and characterization

Ebru A. Buyuktanir [a,*], Margaret W. Frey [b], John L. West [a]

[a] Liquid Crystal Institute, Kent State University, Kent, OH 44242, USA
[b] Fiber Science & Apparel Design, Cornell University, Ithaca, NY 14853, USA

ARTICLE INFO

Article history:
Received 8 June 2010
Received in revised form
2 August 2010
Accepted 8 August 2010
Available online 18 August 2010

Keywords:
Electrospinning
Liquid crystal/polymer composites
Optoelectronic fibers

ABSTRACT

We report here the formation and structural characterization of optically responsive, highly birefringent electrospun nematic liquid crystal (LC) microfibers. The LC microfibers are electrospun from a solution of polylactic acid (PLA) and low molecular weight 4-pentyl-4′-cyanobiphenyl (5CB) in chloroform/acetone solvent. In the electrospinning process, the low molecular weight 5CB phase-separates and self-assembles to form a planarly aligned nematic core within a PLA shell. The solubility limit of 5CB in PLA and the degree of phase separation of LC in the 5CB/PLA core/sheath fibers is determined using the phase transition enthalpies associated with LC and polymer components. Structural analysis revealed that the LC core and dissolved LC in the fibers promote the formation of the α-form of PLA crystals and increase the degree of crystallinity of the PLA shell in 5CB/PLA fibers from 6.6% to 52%. Competition between 5CB droplet formation and PLA fiber formation is observed as a function of spinning solution composition and applied electrospinning voltage. Alignment of the 5CB within the PLA core is confirmed by polarizing optical microscopy.

1. Introduction

LC materials and LC/polymer composites have been extensively utilized in a variety of flexible light modulating devices [1–3]. Recently researchers have prototyped reflective cholesteric liquid crystal displays on fabric substrates by sequential coating of functional layers on a planarized surface [4]. Other display technologies have also been incorporated into fibers, such as light emitting diode (LED) illuminated optical fibers [5] and organic-light-emitting-diode (OLED) coated glass fibers [6]. Nevertheless, most of the previously reported prototypes negatively impact the physical characteristics of textiles by, for instance, reducing flexibility and breathability.

Polymeric liquid crystal materials have been formed into fibers to utilize some of the unique properties, such as mesophase properties, self-ordering at the molecular level, birefringence, and exceptional mechanical properties. The electrospinning of liquid crystalline elastomers has also been studied for potential use as mechanical actuators because of the anisotropic physical characteristics associated with this class of materials [7–9]. The electrospinning of liquid crystalline polysiloxane with a cholesterol side chain and a low molecular weight LC has been reported [10]. No phase separation of polysiloxane and the low molecular weight LC was observed. In other approaches, the solutions of polymers mixed with additives have generally been implemented by a coaxial electrospinning to ensure the partitioning of the small molecules in the core [11], rather than on the surface [12], of the fibers. For example, Lagerwall et al. reported on the coaxial electrospinning of nematic LCs into a poly(vinylpyrrolidone) (PVP)/TiO_2 sheath in order to obtain fibers with a low molecular weight LC core and polymeric shell [13]. In this method, LC material was pumped via a separate channel into the core of the fiber. Even though these previous studies show methods for creating birefringent fibers, they do not provide insight into optical, structural, and morphological characteristics of the core-shell LC microfibers, or the effect of a LC core on the properties of a fiber shell.

Here we successfully demonstrate the self-assembly of low molecular weight liquid crystals in the core of a microfiber during electrospinning. The information obtained from the structural analysis of the fully flexible and electrospun 5CB/PLA microfibers are correlated to the optical properties of fibers. In addition, the optical characterization of the ordered LC fibers provides additional information to show the light modulating properties of the LC fiber arrays. Electrospinning of a homogeneous LC/polymer solution results in highly birefringent and optically responsive LC microfibers. We present the optimization of the optical properties and the morphology of LC fibers by varying the concentration of LC

* Corresponding author. Fax: +1 330 672 2796.
E-mail address: eabuyukt@kent.edu (E.A. Buyuktanir).

0032-3861/$ – see front matter © 2010 Elsevier Ltd. All rights reserved.
doi:10.1016/j.polymer.2010.08.011

material and altering the electrospinning parameters. Polarized optical microscopy (POM) and thermal analysis are used to confirm that 5CB is phase-separated and self-assembled in the core of the PLA at above 28 wt.% 5CB. We also studied how the soft matter properties of 5CB affect the crystallinity of the PLA shell by using wide angle X-ray diffraction (WAXD) and differential scanning calorimetry (DSC).

2. Experimental section

2.1. Materials

Polylactic acid (M_w = 186,000, M_w/M_n = 1.76) was supplied by Cargill Dow LLC (Minnetonka, MN). Chloroform and acetone were purchased from Sigma–Aldrich (St. Louis, MO) and used without further purification. 4-pentyl-4'-cyanobiphenyl (5CB) was obtained from EM Chemicals, Merck.

2.2. Electrospinning process

The electrospinning apparatus is composed of a high-voltage supply (Gamma High Voltage Research Inc., FL), a programmable syringe pump (KDS Model 100), and a collection plate mounted on a stage. The collection plates used in this study include a copper plate, a diamond-shaped Aluminum mesh, an indium-tin-oxide (ITO) coated glass substrate (Corning, 1.1 mm thick), and a cover slip (Fisher Scientific, 0.1 mm thick) attached to the copper plate. The 5 mL glass syringe (Popper Micro-mate) was purchased from VWR Scientific (West Chester, PA). The electrospinning unit was arranged in a horizontal fashion to collect fibers onto a collection plate placed 6 – 16 cm away from the needle tip. The electrospun composite fibers of 5CB/PLA were prepared as follows. First, PLA and 5CB were mixed together, and then chloroform/acetone solvent (3:1 volume ratio) was added. The 5CB/PLA/solvent mixture was mechanically stirred on a plate (Fisher Model 210T) for a day at room temperature. The concentration of PLA in chloroform/acetone solvent was 7.3 wt.% for all samples. Next the polymer solution was drawn into the glass syringe and injected with a metal needle using a syringe pump. Both pure PLA and 5CB/PLA fibers were electrospun with a metallic needle of 24 gauge (0.41 mm in diameter). The electric potential difference (10–22 kV), the collection distance (6–16 cm), and the feeding rate (0.1–1mL/h) were varied to modify the morphology of the composite fibers.

2.3. Characterization of the fibers

The optical textures, morphology, and fiber diameter for the electrospun PLA and composite 5CB/PLA fibers were examined with a polarized optical microscope (POM) (Olympus BX60) after collection onto a glass cover slip (15 × 15 mm). The optical images were captured by MGI Video Wave 4 Software under the crossed polarizers. Morphology and fiber diameter were examined using a Leica 440 SEM at 25 kV. The samples were coated for 30 s with Au–Pd (gold–palladium) using Ar (argon) inert gas plasma prior to imaging. The thermal characteristics of electrospun 5CB/PLA fibers were studied using a Modulated DSC 2920 (TA Instruments) in a nitrogen atmosphere. The electrospun fiber mats were sealed in aluminum pans, and an empty sealed aluminum pan was used as a reference. For all DSC experiments, samples were first cooled down to 10 °C and kept there for 10 min before heating at a rate of 5 °C/min. TA Universal Analysis software was utilized to locate peak maxima for establishing the phase transition temperatures, as well as the enthalpy changes, for these transitions. For DSC characterization, the electrospun 5CB/PLA non-woven mats were collected at 20 kV, 10 cm, and a 0.6 mL/h feeding rate. The concentration of the 5CB was varied from 6.6 wt.% to 86 wt.%. A pure 5CB sample was heated from 10 °C to 75 °C with a 5 °C/min heating rate. 5CB/PLA fiber samples were heated from 10 °C to 190 °C with a 5 °C/min heating rate. WAX diffraction patterns of electrospun 5CB/PLA non-woven fabrics were measured with a Scintag PADX diffractometer scanning from 2Θ = 2–40° at a rate of 3°/min using copper Kα radiation, 45 kV, and 40 mA. %crystallinity of the samples was calculated using JADE 7 software (X-Ray Materials Data, Inc.). Two-dimensional (2D) X-ray diffraction (2DXRD) (Bruker AXS D8 Discover X-Ray) with 2D image processing and 2D diffraction patterns was utilized to characterize 5CB/PLA fibers at elevated temperatures.

3. Results and discussion

3.1. The effect of voltage and the concentration of 5CB on the LC fiber morphology

The concentration of 5CB in PLA was varied from 6.6% to 86% (w/w). Fibers can be formed with up to 70 wt.% 5CB (Fig. 1a). At 86% 5CB the initial solution was very turbid, and did not form a homogeneous solution even after several hours of mixing. Electrospinning

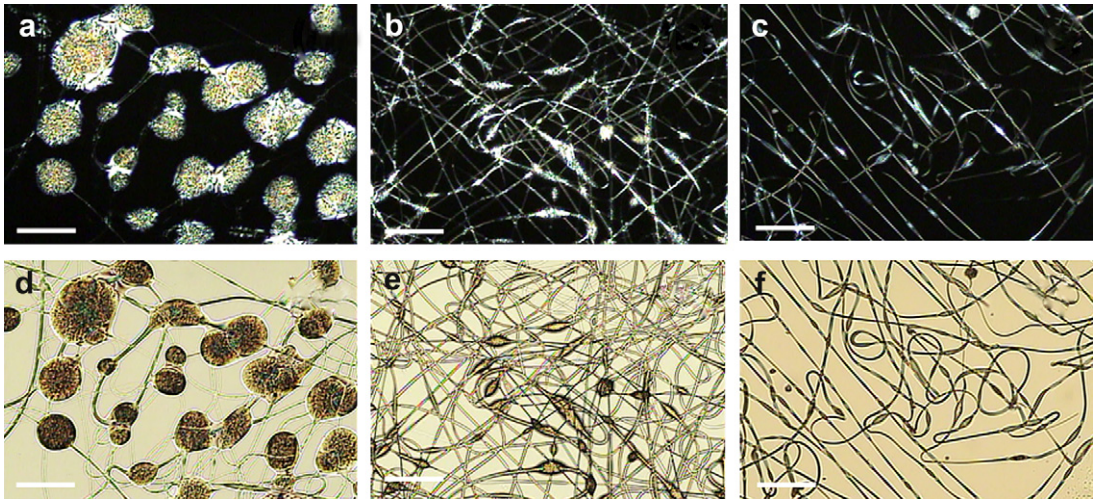

Fig. 1. Effect of the wt.% of 5CB on the morphology of the electrospun 5CB/PLA fibers are shown under crossed polarizers (a–c) and under parallel polarizers (d–f). (a) & (d) 70%, (b) & (e) 58%, and (c) & (f) 40% 5CB. The inset scale bar corresponds to 50 μm. These fibers are collected at 20 kV, 0.6 mL/h, and at 10 cm.

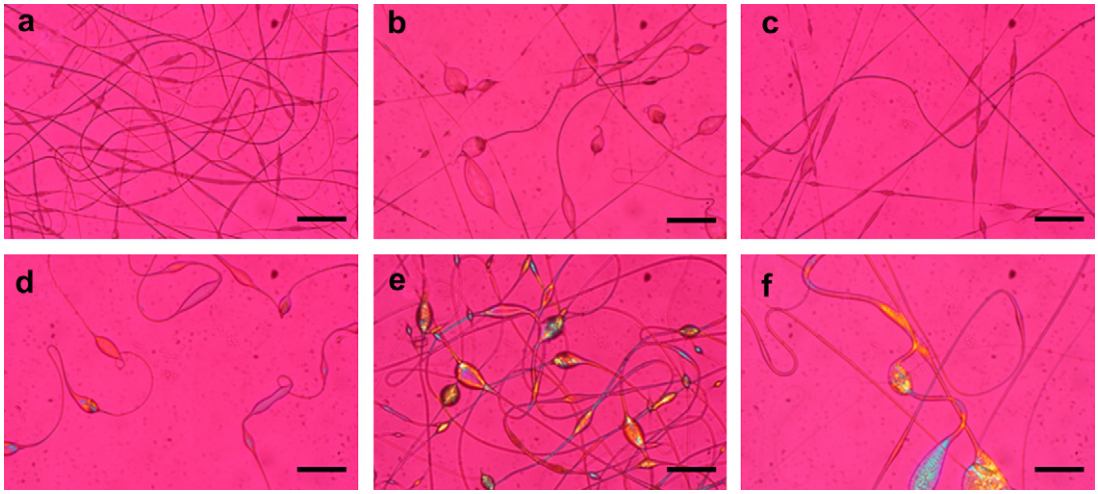

Fig. 2. The birefringence of the 5CB/PLA fibers by utilizing POM equipped with a first order retardation plate (RP). The weight % of 5CB was (a) 0%, pure PLA fibers; (b) 6.6%; (c) 17%; (d) 40%; (e) 58%; (f) 70%. A 530 nm RP was added between the polarizer and analyzer. When the slow axis of RP coincides with the slow axis of LC, it results in the additive retardation and interference color shifts towards shorter wavelengths. Otherwise, the relative retardation decreases and shifts towards longer wavelengths.

of this solution gave rise to "LC-polymer islands" surrounded with nematic 5CB. However, at lower concentrations of 5CB, electrospinning of 5CB/PLA resulted in the formation of beaded and birefringent composite fibers. As shown in POM images in Fig. 1, the optical textures of the electrospun 5CB/PLA core/shell fibers (70–40% 5CB) were examined under both crossed polarizers (Fig. 1a–c) and parallel polarizers (Fig. 1d–f). All the fibers were electrospun with an applied voltage of 20 kV. At 70 wt.% 5CB, electrospinning gave rise to mostly spherical LC droplets and a few very thick birefringent fibers throughout the sample. However, electrospinning of 70% 5CB/PLA at lower voltages (15.5 kV) gave rise to very thick core-shell microfibers (~2.5 μm thick) as well as spherical droplets of LC domains. From OM images shown in Fig. 1a and d, it is clear that the LC material is contained in a polymer shell, although some of the LC material covers the surface of the fibers. As the 5CB ratio decreases, beads also decrease in size, all LC material are contained within the fibers, and the fiber morphology becomes more uniform. Also at 5CB concentrations below 40%, a low overall birefringence is evident with no obvious separation into a highly birefringent core surrounded by a more weakly birefringent shell (Fig. 2a–c). The changes in the birefringence of the fibers were determined by utilizing POM equipped with a first order retardation plate (RP). A 530 nm RP was added between the polarizer and analyzer. At 5CB concentrations of 40% and 58%, however, the 5CB/PLA core/shell structure is obvious, with strong 5CB birefringence evident in the core of both fibers and beads (Fig. 2d–f).

Influence of electrospinning process parameters on the fiber morphology was also explored. Varying the collection distance (6–16 cm) did not result in any significant difference in fiber size, shape, or uniformity (not shown here). The variation in applied voltage (14–25 kV) altered the morphology of the composite LC fibers significantly, as illustrated in the POM images of 58% 5CB fibers in Fig. 3a–e. For these samples, the concentration of 5CB, the feeding rate of the polymer solution, and the collection distance were kept at 58 wt.%, 0.6 mL/h, and 10 cm, respectively. Particularly, the application of higher voltages above the threshold voltage (~14 kV) generated a noticeable change in the size and shape of LC fibers, as shown in SEM images of the fibers in Fig. 4. Voltage drop between the spinning needle and the collector is the major driving force in electrospinning and the increase in voltage drop results in

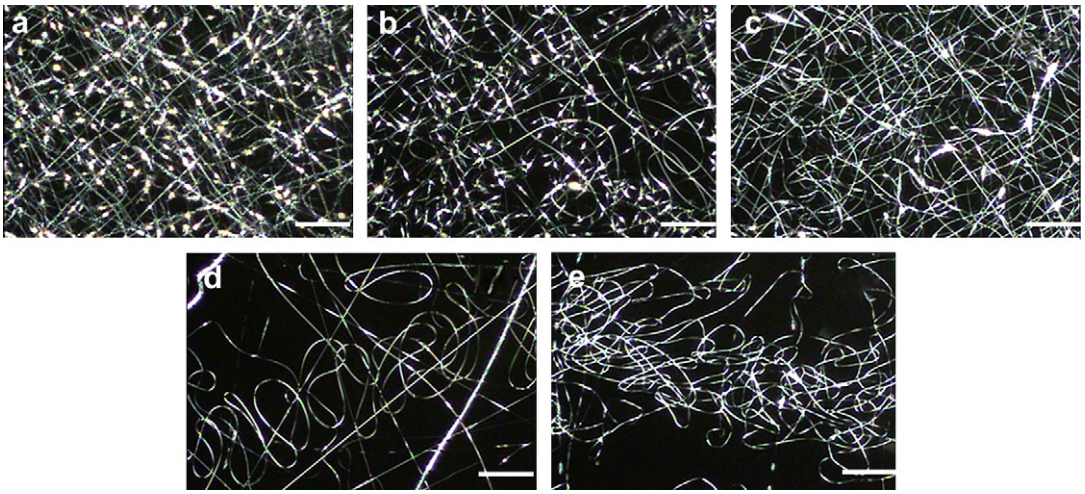

Fig. 3. POM images of 58% 5CB/PLA fibers collected at 0.6 mL/h, 10 cm, (a) 14 kV, (b) 18 kV, (c) 20 kV, (d) 22 kV, and (f) 25 kV. A 10× objective was used and inset scale bars indicate 100 μm.

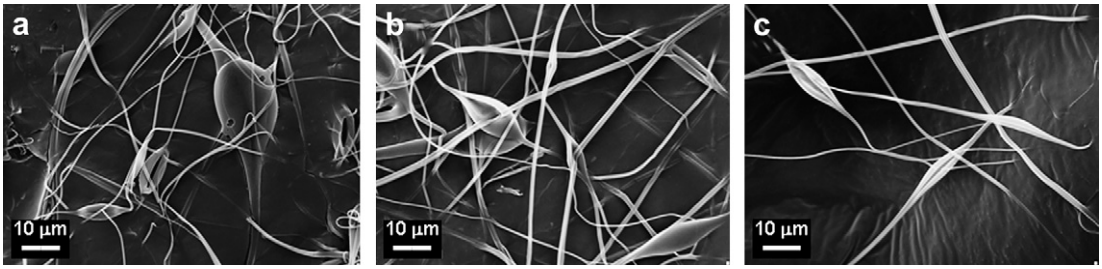

Fig. 4. SEM images of 58% 5CB/PLA collected at 0.6 mL/h, 10 cm, (a) 14 kV, (b)20 kV, and (c) 22 kV.

increasing mass throughput and large fibers. The fiber diameters between beads increased from 500 nm to 2 μm with increasing voltage. Additionally, the competition between surface tension driving the polymer solution to form droplets (aspect ratio ideally 1) and the electrical and rheological forces extending the polymer solution into fibers (aspect ratio infinite) are evident in the change in the bead shape with increased voltage [14]. The length to width ratio of the beads on the fibers increased from approximately 2.0 to 4.0 as the applied voltage was increased from 14 kV to 25 kV. Corresponding SEM images (Fig. 4a–c) confirm both the elongation of the bead shapes and the core/shell structure of the fibers. Fibers and beads have collapsed under vacuum applied in the SEM as 5CB evaporates and leaves behind the PLA sheath. Fig. 5 shows the comparison of 5CB/PLA fibers (Fig. 5a–c) to pure PLA fibers (Fig. 5d–f) that were electrospun at the same conditions. Both PLA and 5CB/PLA fibers have very similar morphologies as the applied voltage is increased from 14 kV to 22 kV; however, the aspect ratio of the beads and the flattening of the beads are quite different, as seen from OM images. The statistical analysis of the aspect ratio and the flattening of the beads and the aspect ratio of the beads are plotted in Fig. 5g, showing that the beads are larger in size and less flat for 5CB/PLA fibers than pure PLA fibers. Likewise, as we increased the applied voltage, the bead size distribution for 5CB/PLA fibers becomes larger than that of pure PLA fibers. (The flattening is $f = (\text{semimajor} - \text{semiminor})/\text{semimajor}$; $f = (a/2 - b/2)/a/2$; the aspect ratio = L = a/b). These results prove that we can easily modify the size and shape, as well as the LC texture, in composite LC fibers by changing the electrospinning parameters.

3.2. Thermal analysis of the LC fibers

Here we probed the temperature dependent first order phase transition characteristics of 5CB confined in the fiber cavities by using DSC. Above the nematic-isotropic phase transition

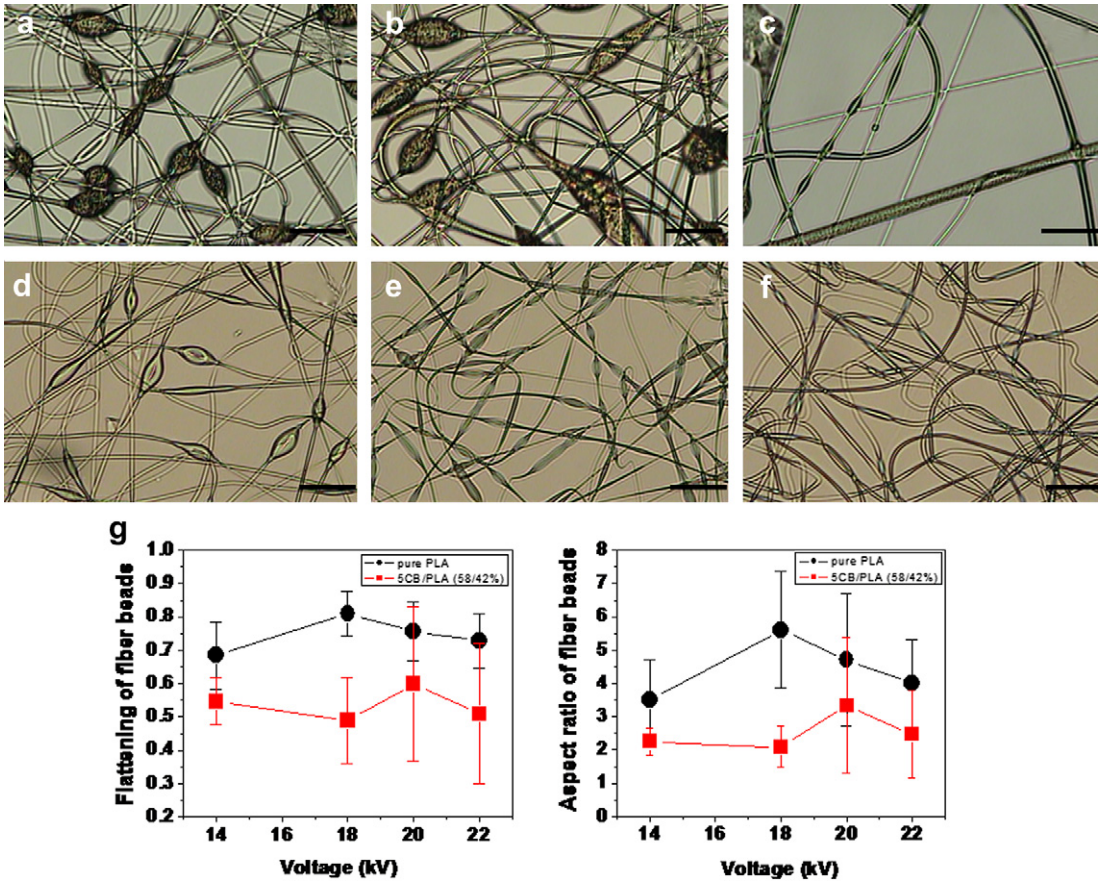

Fig. 5. OM images of electrospun PLA/5CB fibers (top row) and pure PLA fibers (bottom row) collected at 0.6 mL/h, 10 cm, (a)–(d) 14 kV, (b)–(e) 20 kV, and (c)–(f) 22 kV and shown under parallel polarizers. (g) The degree of flattening "*f*" and the aspect ratio "*L*" of the beads of electrospun fibers versus applied voltage.

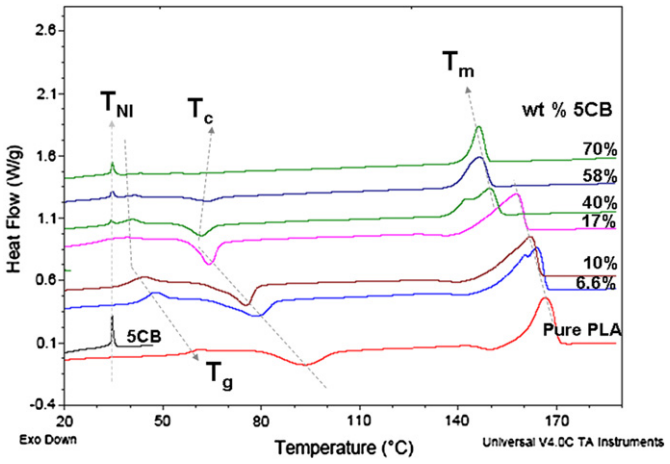

Fig. 6. DSC curves for pure 5CB, pure PLA, and 5CB/PLA non-woven fabrics. The weight percent of 5CB was varied from 0 to 70%. Dashed lines indicate the nematic-isotropic phase transition (T_{NI}), the glass transition (T_g), the cold crystallization (T_c), and the melting (T_m) peaks.

temperature ($T_{NI} \sim 35$ °C for 5CB), 5CB is an isotropic liquid. The DSC thermographs for electrospun 5CB/PLA fibers, pure PLA fibers, and pure 5CB are shown in Fig. 6. The effect of PLA on T_{NI} is plotted in Fig. 7a. Above 40% 5CB in fibers, T_{NI} does not change, indicating that the nematic LC mesophase completely phase-separated and self-assembled in the cavities of PLA shell. On the other hand, below 40% 5CB, T_{NI} for 5CB/PLA fibers was lower than that of pure 5CB. The depression of T_{NI} likely results from trace amounts of solvents or polymer present in the cavities of the fiber. The plot in Fig. 7a intercepts the *x*-axis at 28.8% 5CB, which can be taken as the liquid crystal solubility limit "*A*" in PLA. Below 30% of 5CB, we did not obtain any T_{NI} peak.

The DSC thermograph of a pure electrospun PLA fiber mat shows the endothermic glass transition ($T_g \sim 59$ °C) and the exothermic cold crystallization peak ($T_c \sim 93$ °C), followed by the endothermic melting transition ($T_m \sim 167$ °C) of PLA [15]. Fig. 7b–d shows the T_g, T_c, and T_m of the 5CB/PLA fibers with respect to the weight percent of 5CB. In the presence of 5CB in the PLA fiber structure, the T_g, T_c, and T_m of pure PLA fibers are depressed by 17.6 °C, 30 °C, and 20.4 °C, respectively, as the LC content is increased from 0% to 70% in the fibers. The onset of T_g was calculated using the half-step method [16]. As the fraction of 5CB is increased up to the solubility limit (~28%) in PLA, T_g declines linearly, suggesting that the dissolved LC material enhances the segmental molecular mobility of PLA. However, as the nematic mesophase of 5CB phase-separates at concentrations above 28% in the core of the fiber, T_g increases by 7–10 °C. T_c appears due to the existence of crystallizable free amorphous regions of electrospun PLA fibers. In 5CB/PLA fiber mats, it is observed that T_c decreases almost linearly up to 28% 5CB, and then becomes almost constant, even at the highest load of 70% 5CB. The decrease in T_c can be attributed to the heterogeneous nucleation of PLA in the presence of 5CB. The T_c value of PLA continues to decline as the 5CB content is increased within the fibers until the 5CB solubility limit is reached. Similar heterogeneous nucleation affects on PLLA crystallization have been observed in PLLA/Polycaprolactone blends with limited miscibility [17]. Only T_m continues to decline without reaching a plateau. The steady decrease in T_m indicates the formation of smaller, but less organized and imperfect, PLA crystalline structures. This type of behavior in electrospun PLA systems was previously reported by Zhou et al. [15]. Heck et al. also reported a detailed study on the effect of low-molar-mass diluents on the melting point depression

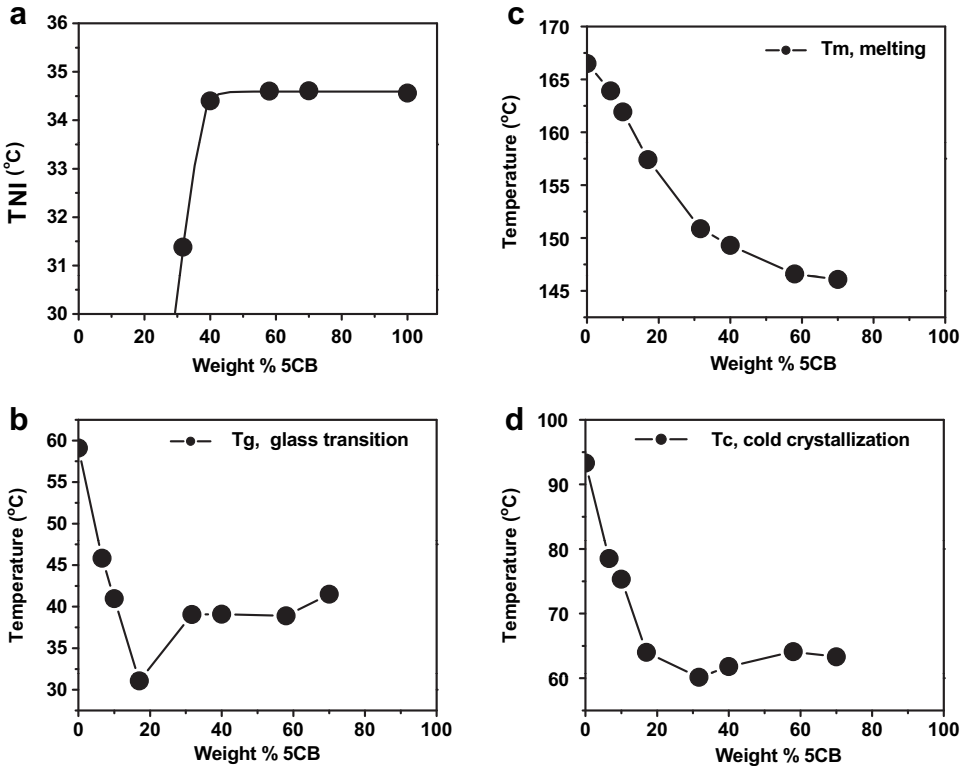

Fig. 7. (a) Dependence of T_{NI} on the weight % of 5CB. Dependence of (b) T_g, (c) T_m, and (d) T_c of PLA on the weight % of 5CB in the 5CB/PLA non-woven fabrics.

and the polymer crystallization [18]. They found that polymer crystallization is a multi-stage process and the crystal thickness is largely affected in the presence of diluent molecules, leading to intermediate mesomorphic phase.

The value of A was also found by using the nematic-isotropic enthalpy (ΔH_{NI}) derived from DSC thermographs (Fig. 6) for composite fibers with a phase transition peak. Fig. 8a illustrates the linear dependence of ΔH_{NI} with respect to the weight% of 5CB of fiber mats. The ΔH_{NI} values were corrected for the weight fractions of 5CB present in the mixtures of 5CB/PLA. Both the value of A and the fraction of phase separated LC (f) were calculated based on the Equations (1)–(3) reported by Smith et al. [19]. Russell et al. [20] also utilized the same approach to analyze polymer dispersed liquid crystal (PDLC) systems prepared by a polymerization-induced phase separation method.

The relationship between the nematic-isotropic enthalpy of mixtures $\Delta H_{NI}(X)$ and the enthalpy of pure liquid crystal $\Delta H_{NI}(LC)$ is given as follows,

$$\frac{\Delta H_{NI}(X)}{\Delta H_{NI}(LC)} = \frac{X - A}{100 - A} \tag{1}$$

in which X is the weight percent of LC in 5CB/PLA fibers. The fraction of phase separated LC material f in these systems was calculated first by using Eq. (2),

$$\phi = \frac{100}{X}\frac{\Delta H_{NI}(X)}{\Delta H_{NI}(LC)} \tag{2}$$

φ can also be expressed by combining Eq. (1) and Eq. (2),

$$\phi = \frac{100}{X}\frac{(X - A)}{(100 - A)} \tag{3}$$

Using Eq. (3), f was next calculated and plotted with respect to X, as in Fig. 8b. The A value was found as 28.2 wt.% 5CB by a linear fit and extrapolating the data to zero. Although dissolved LC in PLA does not contribute to ΔH_{NI}, the value of f and ΔH_{NI} increase with LC concentration, as plotted in Fig. 8a and b, respectively. The value of f depends on temperature, as well as the solubility parameters of the polymer matrix and LC. It is desirable to choose a polymer with a solubility parameter that is different than that of LC core in order to increase the phase separated LC amount in the core.

3.3. WAXD results and crystallinity

In addition to DSC, the structural changes induced by 5CB in the PLA fibers were measured utilizing a WAXD technique in order to identify the degree of polymer chain ordering in the crystalline lamellae and the types of crystals formed in PLA fibers in the presence of 5CB. The results of the WAXD shown in Fig. 9a confirm that the PLA crystal growth in fibers is affected by the phase separated 5CB. The PLA crystallization in the presence of the orientationally ordered LC phase indicates that the phase separated liquid crystal domains enhance the nucleation process or act as heterogeneous nucleation sites for amorphous PLA chains. A strong crystalline peak at $2\theta = 16.9^\circ$ and a smaller peak at $2\theta = 19.2^\circ$ appeared in the WAXD patterns of the composite fiber mats when the LC content was above 30%. These peaks are consistent with the α-crystalline polymorph of PLA, as previously reported [21–23]. On the other hand, only a broad peak is observed for lower concentrations of electrospun 5CB/PLA and for pure PLA non-woven fabrics. The α-form of PLA crystal is characterized by antiparallel chains packed in an orthorhombic unit cell with lamellar folded chain morphology. The detailed information about the α-form of PLA can be found in a comprehensive review by Pan et al. [24]. It is clear that both dissolved LC and the LC core in PLA fibers promote the formation of three dimensional ordered crystallites.

The intensity of the diffraction peak of PLA also increased with increasing LC content. The %crystallinity (χ) for each 5CB/PLA sample was obtained from DSC and WAXD data and plotted in Fig. 9b. WAXD data analysis shows that the orientationally ordered nematic phase modifies the crystallization process of PLA and increases the crystallinity of the fibers up to ~52% in the presence of 70% 5CB. %χ was calculated per gram of PLA present in these samples by dividing the χ value of 5CB/PLA fiber mat by the weight fraction of PLA. Likewise, by utilizing the enthalpies for cold crystallization ΔH_c and melting ΔH_m from DSC curves, the apparent crystallinity is calculated from Eq. (4). Both ΔH_c and ΔH_m are normalized to the PLA weight fraction in the fiber mats. %χ is given as,

$$\chi(\%) = \frac{\Delta H_m - \Delta H_c}{\Delta H_f} \times 100 \tag{4}$$

where ΔH_f is the heat of fusion for 100% crystalline PLA, and its value is reported as 93.1 J/g [25,26]. Even though the interaction of the 5CB core with PLA lowers the T_m value of PLA, the apparent degree of crystallinity of PLA increases dramatically from 16% (pure PLA) to 54% (70% 5CB).

No distinct peaks, only diffuse spots, have been reported for WAXD measurements of 5CB in the nematic phase due to lack of long-range positional order [27,28]. Even though the surface-induced smectic layering in confined systems has been observed only in LC materials possessing a smectic phase with quasi-long range positional order in 2D [29], we wanted to confirm our findings at elevated temperatures. In addition to WAXD, we utilized

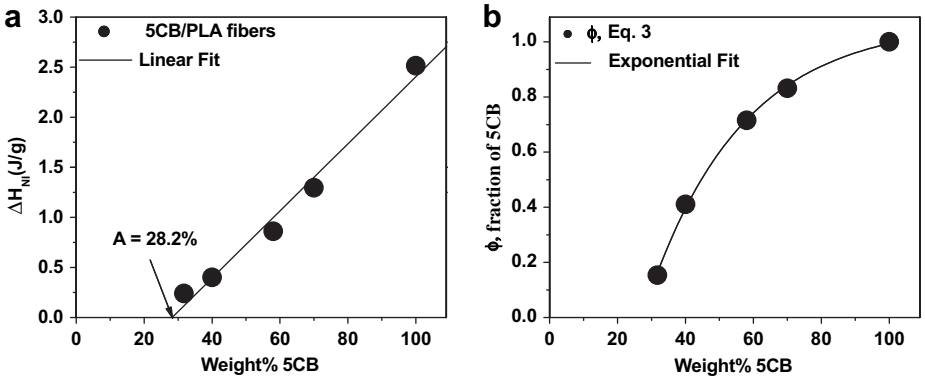

Fig. 8. (a) Dependence of ΔH_{NI} (the nematic-isotropic enthalpy) on the weight % of 5CB in the 5CB/PLA nonwoven fabrics. (b) The fraction of phase separated LC material (φ) versus the weight % of 5CB in the 5CB/PLA non-woven fabrics. f is calculated based on Eq. (3).

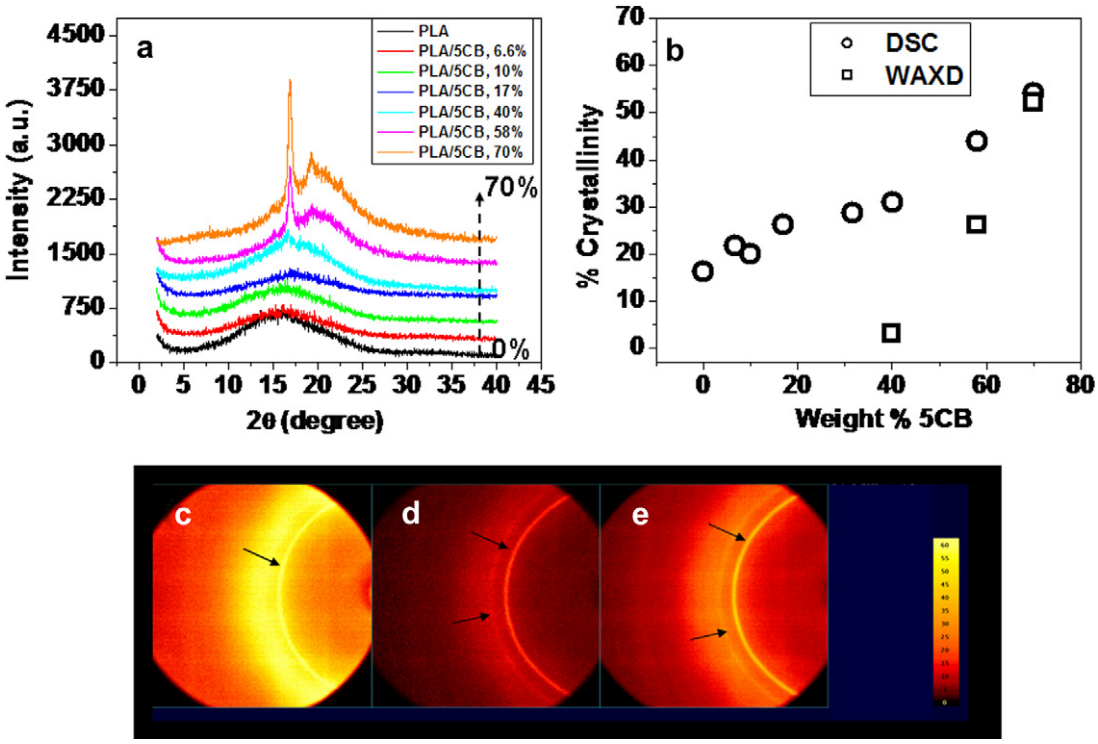

Fig. 9. (a) Wide angle X-ray diffraction patterns for the electrospun pure PLA and the composite 5CB/PLA non-woven fabrics. The weight % of 5CB was varied from 0% to 70%. (b) The plot of apparent degree of crystallinity based on DSC curves and WAXD data versus the weight % of 5CB. (c)–(d) 2DXRD maps collected for a 5CB/PLA (70/30 wt.%) fiber mat: (c) at room temperature after 5 min; (d) at 70 °C after 1 min; (e) at 70 °C after 5 min data collections. Arrows on the images point to the crystallization peaks of PLA. The area detector displays the two-dimensional diffraction pattern into a two-dimensional image frame with a color scale.

a 2DXRD technique to study 5CB/PLA fiber mats at above T_{NI} to observe the LC mesophase effects on the crystallization peaks of PLA. As illustrated in Fig. 9c, the 5CB/PLA fiber (70/30 wt.%) mat contains a crystallization peak on the 2D X-ray diffraction map at room temperature without any heat treatment. Later we heated the sample up to 70 °C, at which 5CB is isotropic liquid, and scanned the sample again. As seen in Fig. 9d and e, after 1 min and 5 min of data collections, respectively, the composite non-woven fabric still

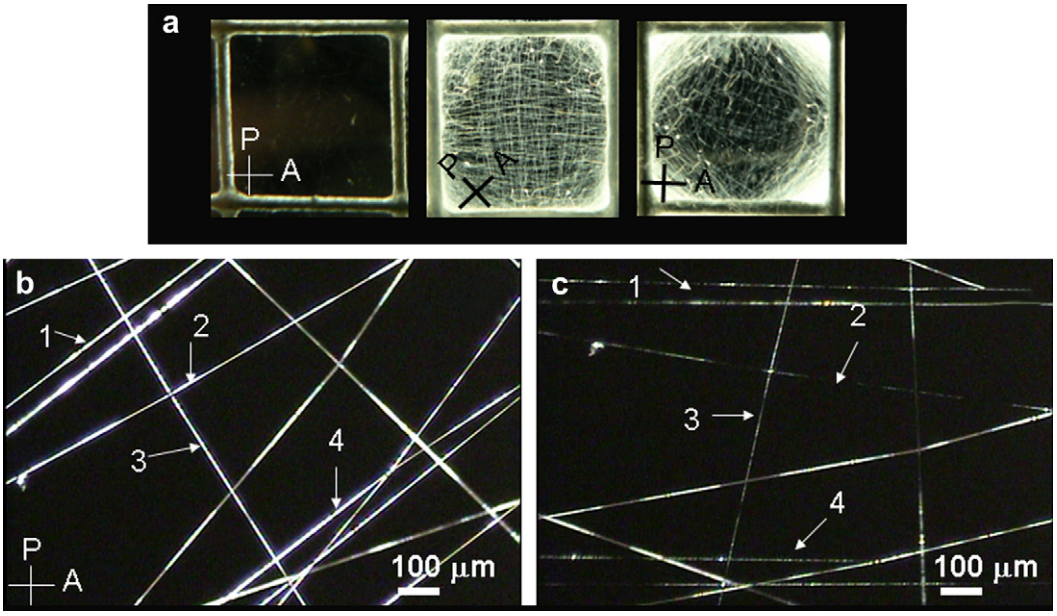

Fig. 10. The polarized optical microscopy images of the uniform and the beaded electrospun 5CB/PLA (58/42 wt.%) fibers collected at (a) 25 kV and (b) 14 kV, respectively. (c) The same fibers are collected onto a metal grid and the pictures of the oriented LC fiber array that is rotated between crossed polarizers. (d) POM images of the birefringent and ordered 5CB/PLA fibers rotated under crossed polarizers until the polarized light is blocked by the fibers 1 to 4 shown by arrows. 20× and 5× microscope objectives are used.

showed the crystallization peaks. This result proves that the composite fabrics possess significant PLA crystallinity, which is induced during the electrospinning process.

However, it is not clear how the long-range orientational order existing in nematic 5CB induces a high degree of crystallinity (~52%) to almost amorphous PLA. Based on our thermal analysis, we found that dissolved LC increased the segmental mobility of PLA, and, therefore, the increased PLA crystallinity may partially be the result of solvent-induced crystallization due to the lowered T_g. In fact, several groups reported on the improved crystallization of PLA matrix through solvent penetration or by addition of particles [22,26]. For instance, PLA immersed in ethanol gave rise to ~15% crystallinity in one study [30]. An extensive study reported by Xiao et al. [31] on the effect of plasticizers on PLA crystallization shows that the diffraction peaks of PLA decrease in the presence of plasticizers when compared to the neat PLA. Hence, the increase in the intensity of the peaks in 5CB/PLA fiber mats cannot be explained only by the plasticizing effect of LC medium. The long-range orientational order in LC mesophase may act as a nucleating site and enhance the crystallization by providing an ordered interface for the growth of PLA crystals.

3.4. Light modulating LC fiber arrays

The anisotropic optical properties of LCs are the basis for their ability to change the polarization state of light [32]. The electrospinning of the 5CB/PLA solutions resulted in the formation of highly birefringent and light modulating micrometer size LC fibers at room temperature. Since 5CB is a positive birefringent material ($\Delta n \sim 0.2$ at 25 °C), the nematic phase in the 5CB/PLA fibers can be recognized from typical LC optical textures as we have shown previously. In these optical textures, the spatial variation in light intensity depends on the phase shift and the in-plane director configuration [33]. On the other hand, electrospun PLA fibers appear completely dark under crossed polarizers because of the PLA's very low optical anisotropy ($\Delta n \sim 0.03$) [25]. The ordered fiber array collected on a metal grid shows the polarization sensitivity of the fibers (Fig. 10a). Fig. 10b and c show the effect under POM indicating that 5CB is planarly aligned within the core of PLA shell, and, as we rotate the sample, the linearly polarized light passing through the fibers is either blocked or transmitted, depending on the orientation of the fibers.

4. Conclusion

In this study, we produced and characterized the electrospun 5CB/PLA microfibers composed of phase-separated and self-assembled optically active nematic LC domains. The morphology of the fibers was optimized to obtain uniform light modulating LC fibers by varying the electrospinning parameters. As a result, the optical birefringence of the liquid crystal core couples with the cylindrical structure of the PLA shell and forms the optically responsive 5CB/PLA composite microfibers. The optical birefringence and dielectric anisotropy of liquid crystals couples with the elongated structure of the polymer shell to form the basis of the light modulating properties of the LC fibers. Thermal analysis and WAXD results showed that both dissolved and phase separated 5CB promote the PLA crystallinity significantly. The present study provides a foundation for further formulation and optimization of highly birefringent and stimuli-responsive composite LC fibers. Ultimately, these results may contribute to the development of non-woven optoelectronic textiles, ranging from sensors to displays.

Acknowledgements

The authors would like to thank the Burton Morgan Foundation and Flexible Liquid Crystal Film Manufacturing Alliance, Ohio Department of Development (Grant# 444205) for financial support. The authors would also like to thank Dr. Elizabeth Rhodes, Dr. Miko Cakmak, Wei Zhao, and Erin Hendrick for their help in this project.

References

[1] Büyüktanır EA, Gheorghiu N, Mitrokhin M, Holter B, West JL, Glushchenko A. Appl Phys Lett 2006;89(3):031101.
[2] Stephenson SW, Johnson DM, Kilburn JI, Mi X-D, Rankin CM, Capurso RG. SID Int Symp Dig Tech Pap 2004;35:774.
[3] West JL, Zhang K, Zhang M, Buyuktanir EA, Glushchenko A. Proc SPIE 2005;5936:59360L.
[4] Khan A, Shiyanovskaya I, Schneider T, Doane JW. SID Int Symp Dig Tech Pap 2006;37:1728.
[5] Koncar V. Opt Photonics News 2005;16(4):40.
[6] Yase K, Suzuki K, Hiroshima M, Mimura A, Shuu YM, Toda S, et al. SID Int Symp Dig Tech Pap 2006;37:1870.
[7] Canejo JP, Borges JP, Godinho MH, Brogueira P, Teixeira PIC, Terentjev EM. Adv Mater 2008;20(24):4821–5.
[8] Krause S, Dersch R, Wendorff JH, Finkelmann H. Macromol Rapid Commun 2007;28:2062–8.
[9] Palffy-Muhoray P. Nat Mater 2009;8:614–5.
[10] Wu Y, An Q, Yin J, Hua T, Xie H, Li G, et al. Colloid Polym Sci 2008;286:897–905.
[11] Zhang YZ, Wang X, Feng Y, Li J, Lim CT, Ramakrishna S. Biomacromolecules 2006;7:1049–57.
[12] Sanders EH, Kloefkorn R, Bowlin GL, Simpson DG, Wnek GE. Macromolecules 2003;36(11):3803–5.
[13] Lagerwall JPF, McCann JT, Formo E, Scalia G, Xia Y. Chem Commun; 2008:5420–2.
[14] Jacobs V, Anandjiwala RD, Maaza MJ. Appl Polym Sci 2010;115(5):3130.
[15] Zhou H, Green T, Joo YL. Polymer 2006;47:7497–505.
[16] Turi EA. Thermal characterization of polymeric materials. 2nd ed. San Diego: Academic Press; 1997.
[17] Sakai F, Nishikawa K, Inoue Y, Yazawa K. Macromolecules 2009;42:8335–42.
[18] Heck B, Strobl G, Grasruck M. Eur Phys J E 2003;11:117–30.
[19] Smith GW, Ventouris GM, West JL. Mol Crys Liq Cryst 1992;213:11–30.
[20] Russell GM, Paterson JAB, Imrie CT. Chem Mater 1995;7:2185–9.
[21] Lopez-Periago A, Garcia-Gonzalez CA, Domingo CJ. Appl Polym Sci 2009;111(1):291–300.
[22] Xiang C, Joo YL, Frey MW. J Biobased Mater Bioenergy 2009;3(2):1–9.
[23] Zhang J, Duan Y, Sato H, Tsuji H, Noda I, Yan S, et al. Macromolecules 2005;38:8012–21.
[24] Pan P, Inoue Y. Prog Polym Sci 2009;34:605–40.
[25] Ou X, Cakmak M. Polymer 2008;49:5344–52.
[26] Lim L-T, Auras R, Rubino M. Prog Polym Sci 2008;33:820–52.
[27] Pople JA, Mitchell GR. Liquid Crystals 1997;23(4):467–73.
[28] Collings PJ. Phase structures and transitions in thermotropic liquid crystals. In: Collings PJ, Patel JS, editors. Handbook of liquid crystal research. New York: Oxford University Press; 1997. p. 99–124.
[29] Crawford GP, Doane JW, Zumer S. Polymer dispersed liquid crystals:nematic droplets and related systems. In: Collings PJ, Patel JS, editors. Handbook of liquid crystal research. New York: Oxford University Press; 1997. p. 347.
[30] Kobashi K, Villmow T, Andres T, Haubler L. Smart Mater Struct 2009;18:035008.
[31] Xiao H, Lu W, Yeh J-T. J Appl Polym Sci 2009;113:112–21.
[32] Büyüktanır EA, Zhang K, West JL, Gericke A. Mol Cryst Liq Cryst 2008;487(1):39–57.
[33] Kleman M, Lavrentovich OD. Soft matter physics: an introduction. New York: Springer-Verlag; 2003.